RESEARCH ARTICLE

Comparing patterns of hurricane washover into built and unbuilt environments

Eli D. Lazarus[a1], Evan B. Goldstein[b1], Luke A. Taylor[a], Hannah E. Williams[a]

[a]Environmental Dynamics Lab, School of Geography and Environmental Science, University of Southampton, Southampton, SO17 1BJ, UK

[b]Department of Geography, Environment, and Sustainability, University of North Carolina at Greensboro, Greensboro, NC, USA

ORCiDs:

EDL: 0000-0003-2404-9661

EBG: 0000-0001-9358-1016

LAT: 0000-0002-2132-4261

HEW: 0000-0002-6143-2523

Correspondence to – Eli D. Lazarus (email: E.D.Lazarus@soton.ac.uk; Twitter: @envidynxlab), Evan B. Goldstein (email: ebgoldst@uncg.edu; Twitter: @ebgoldstein)

Keywords – hurricane, tropical cyclones, overwash, washover, morphometry, distortion

Key points –

- We measure geometric characteristics of sandy washover deposits in built and unbuilt coastal environments following hurricane strikes.
- We quantify systematic similarities and differences between washover morphology in built and unbuilt environments.
- Our findings suggest that the "fabric" of the built environment exerts a fundamental control on large washover deposit form.

Abstract

Extreme geohazard events can change landscape morphology by redistributing huge volumes of sediment. Event-driven sediment deposition is typically studied in unbuilt settings – despite the ubiquity of occurrence and high economic cost of these geohazard impacts in built environments. Moreover, sedimentary consequences of extreme events in built settings tend to go unrecorded because they are rapidly cleared, at significant expense, from streets and roads to facilitate emergency response. Reducing disaster costs requires an ability to predict disaster impacts, which itself requires comprehensive measurement and study of the physical consequences of disaster events. Here, using a database of post-storm aerial imagery, we measure plan-view geometric characteristics of sandy washover deposits in built and unbuilt settings following five different hurricane strikes along the Atlantic and Gulf Coasts of the US since 2011. We identify systematic similarities and differences between washover morphology in built and unbuilt environments, which we further explore with a simplified numerical model. Our findings suggest that the fabric of the built environment – specifically, the built fraction of the depositional zone – exerts a fundamental control on the form of large deposits. Accounting for the influence of the built fabric on the morphodynamics of flow-driven geohazards is a tractable step toward improved forecasts of hazard impacts and disaster risk reduction.

Plain-language Summary

Many kinds of hazardous extreme events – floods, landslides, volcanic activity – send flows laden with sediment coursing into built environments. For example, when hurricanes strike built-up areas of low-lying coastline, huge volumes of sand get channeled down streets and between buildings, requiring expensive emergency clean-up. Patterns of deposition in the fabric of built settings have been described but rarely measured for hurricanes. We measure hurricane deposits in built and unbuilt environments and find systematic similarities and differences between the two types of setting. Our findings suggest that assessment and mitigation of disaster risk in built environments prone to flow-driven hazards could be improved by accounting for the effect of built fabric on sediment dynamics.

1 Introduction

Extreme events such as storms, floods, landslides, and volcanic eruptions can redistribute huge volumes of sediment in landscape systems. These geomorphic impacts tend to be studied in landscapes with minimal human presence, infrastructure, or intervention, to reduce confounding factors on sediment transport. However, human domination of natural environments means that unbuilt conditions now represent exceptional circumstances (Ellis & Ramankutty, 2008; Foley et al., 2005; Halpern et al., 2015; Venter et al., 2016; Vitousek et al., 1997). Moreover, built environments are ubiquitous in hazard-prone settings world-wide. According to the global Emergency Events Database (EM-DAT), since 1970, a total of over 12,000 recorded natural disaster events have affected, on average, more than 150 million people each year – and occasionally several times that number. Economic damage from those disasters totals approximately US$ 4.5 trillion (adjusted to 2019 US$), or an average of nearly US$ 91 billion annually. Reducing disaster costs requires, among other capacities, an ability to predict disaster impacts – which itself requires comprehensive measurement and study of the physical consequences of disaster events. Buried in the global figures for disaster damage, for example, are the costs associated with removing debris from built environments – debris that can include, in any given event, hundreds of thousands to tens of millions of cubic meters of sediment (Brown et al., 2011; EPA, 2019; FEMA, 2020; Lipton, 2013; Periathamby et al., 2012).

A growing body of research into hazard systems – specifically those that involve sediment deposition – is revealing how extreme events interact with built and unbuilt environments in fundamentally different ways. Examples of this divergence tend to be more qualitative than quantitative, but come from a diverse range of hazard types: floods (Nelson & Leclair, 2006), coastal storms (Hall & Halsey, 1991; Nordstrom, 2004; Rogers et al., 2015; Smallegan & Irish, 2017), tsunamis (Bricker et al., 2015; Park et al., 2013), landslides and debris flows (Del Ventisette et al., 2012; Papathoma-Köhle et al., 2017), and volcanic eruptions – both modern (Doronzo & Dellino, 2011) and historical (Gurioli et al., 2005, 2007; Zanella et al., 2007). Systematic, quantitative comparison of event-driven deposition in built and unbuilt settings requires collating characteristics of sediment deposits across different locations, events, and hazard systems. Such a synthesis of morphological characteristics in extreme-event deposits is an empirical step toward prediction of impacts, understanding disaster risk, preparing for disaster response, and risk reduction in built environments prone to geomorphic hazard – in alignment with key goals of the UN Sendai Framework for Disaster Risk Reduction (UN, 2015).

Here, we quantify morphological characteristics of sediment deposits from tropical cyclone strikes along the low-lying and extensively developed Atlantic and Gulf coastlines of the US. During the past four decades, the intensity of tropical cyclones globally has increased (Kossin et al., 2020). In the US, since the 1970s, population has grown disproportionately in coastal counties (NOAA, 2013) and hurricane strikes have become more damaging (Grinsted et al., 2019). On sandy coastlines like the US Atlantic and Gulf, a geomorphic signature of extreme coastal storms is washover deposits – fans or sheets of sediment transported onto the subaerial coastal plain by elevated water levels and shallow overland flow. Washover is constructional: as the main contributor to the subaerial sediment budget of low-lying coastlines, washover regulates the elevation of coastal barrier environments relative to sea level (FitzGerald et al., 2008). Most geomorphic investigations of coastal storm deposition consider unbuilt environments (Donnelly et al., 2006; Engelstad et al., 2017, 2018; Hudock et al., 2014; Lazarus, 2016; Lazarus & Armstrong, 2015; Leatherman & Zaremba, 1987; Masselink & van Heteren, 2014; Matias et al., 2009; Morton & Sallenger, 2003; Shaw et al., 2015; Wesselman et al., 2018). A few notable exceptions have measured washover extent (Hall & Halsey, 1991; Morton & Paine, 1985) and volume (Overbeck et al., 2015; Rogers et al., 2015; USGS 2005) in beachfront built environments following a storm event, or described the phenomenon in built settings more broadly (Nordstrom, 2004). One reason for this dearth of investigations in built environments is that storm deposits in built areas are rapidly cleared away by road crews (Nelson & Leclair, 2006; Nordstrom, 2004) – sometimes even as the storm and deposition is in progress (Lazarus & Goldstein, 2019). Post-storm aerial or satellite imagery may serve as the only record of deposition patterns (**Fig. 1**). These deposits are ephemeral, yet they are fundamental to predicting impacts of future extreme storms, gaining an accurate accounting of sediment budgets in coastal built environments, and finding ways to reduce the burdensome economic costs of post-storm clean-up.

In this analysis, we measure the length, perimeter, and area of individual washover deposits in built (n = 167) and unbuilt (n = 115) settings (**Fig. 2a**), captured by aerial imagery (National Geodetic Survey, 2020) following five different hurricane events along the Atlantic and Gulf Coasts of the US: Irene (2011), Sandy (2012), Matthew (2016), Nate (2017), and Michael (2018) (**Fig. 2b**). We examine and compare scaling relationships in deposit geometry across both built and unbuilt settings, and explore the effect of spatial characteristics – termed "fabric" – of the built environment on washover morphology. Numerical experiments from a deliberately simplified numerical model of washover align with and expand upon our empirical results.

2 Methods

2.1 Empirical measurements

We identified washover deposits visible in geolocated, orthorectified post-storm aerial imagery from NOAA (NGS, 2020), captured within days of hurricane strikes on the US Atlantic and Gulf Coasts. Washover footprints in built and unbuilt settings were digitized manually by the same person using ArcGIS Pro. All data were projected in the NAD 1983 coordinate system. Perimeter and area of each deposit were calculated automatically. Length, taken as the longest orthogonal distance between the seaward and landward edges of the deposit, was determined manually using the Measure tool. In cases where interior portions of a deposit had already been cleared from roads, deposit extent was discerned from plowed ridges of sand evident at roadway margins.

To quantify the fabric of the built environment, building footprints were extracted from the open-access dataset of US building footprints published by Microsoft (https://github.com/microsoft/USBuildingFootprints), and OpenStreetMap street networks downloaded from Geofabrik (https://download.geofabrik.de/). The JSO-to-Feature-Class tool in ArcGIS was used to convert each state-level GeJSON file of building footprints into a usable format for ArcGIS. Convex-hull bounding boxes were applied to washover deposits in built settings to capture buildings interacting with a deposit edge, along with any buildings fully enveloped by a deposit (**Fig. 2a**). With the Intersect tool in ArcGIS, building footprints and street networks were clipped by the convex-hull bounding boxes around each deposit to calculate the total (two-dimensional) building area and total street length present within each bounding box.

In built settings, washover perimeter was taken as the outer perimeter of a deposit, and thus excludes the perimeter of any interior geometry created by fully enveloped buildings. Deposit area excludes the area of any buildings interior to (or otherwise interacting with) the deposit. Built fraction was calculated as the total area of building footprint within a convex-hull bounding box, divided by the area of the bounding box. Street length was calculated as the total linear length of street network within a deposit footprint.

2.2 Numerical model

To systematically explore generic patterns of washover deposition into built environments, we adapted a simplified numerical model of washover deposition, described in full by Lazarus and

Armstrong (2015), to include generic fabrics for a range of built fractions. (The model code, written in MATLAB, is available at [https://github.com/envidynxlab/Model-World]) The structure of the numerical model is cellular. One edge of the model domain (here, 100 x 100 cells) is an erodible barrier of height $z = 1$. Initial water height on the "seaward" side of the barrier is set equal to barrier height. The floodplain on the "landward" side of the barrier is topographically flat, but built areas are added as a regular grid of non-erodible blocks of arbitrary height $z = 2$ (to ensure no overtopping). Built footprints are square, and are expanded incrementally over successive trials by increasing the edge length of built squares by one cell. Streets between built squares are held to a constant width of 4 cells. This configuration of the built environment is not intended to simulate a particular locale, only to capture a range of built fractions.

Each domain condition is trialed 25 times. Each trial uses a different breach location, randomly selected from within the middle 60 cells of the barrier edge (to avoid edge effects), and a different breach size, randomly selected as a proportion of barrier height between 0.1–0.7. Varying breach size produces a variety of deposit sizes for a given domain. Cross-shore overwash flow (from the seaward edge of the domain landward) occurs when water height exceeds barrier height. Water set-up against the barrier is treated as a conserved quantity, such that water height along the barrier is lowered at each time step by the volumetric loss from overwash discharge through the breach. Sediment from the barrier is moved as a proportion of flow depth at a given cell; we include a threshold depth required to move sediment. Flow depth at a given cell is distributed proportionally to all neighboring cells of lower elevation, leaving behind a sediment lag (as a proportion of flow depth). In this way, a washover deposit fans into the floodplain domain from the barrier. For configurations in which the built fraction is null or low, breach size and deposit size are positively correlated. As built fraction increases, so does the likelihood that washover at a given breach site will be blocked by a built structure. Randomizing breach locations means that in some trials washover finds open pathways between built areas, and in others gets blocked by an element of the built environment, collectively producing a wide range of possible washover sizes for a given breach size and floodplain configuration.

Each trial runs for a fixed duration of 20 iterations. The number of iterations is nominally analogous to storm duration, but here is set for convenience: the bulk of the washover deposit forms rapidly, within a few iterations, and stops growing once overwash flow depths over its topography are too shallow to move any more sediment. Here, limiting the duration to 20 iterations also ensures that the largest deposits do not flow off the far landward edge of the domain when built fraction = 0. The model domain is not scaled to match length scales in the empirical data (the areas of our modeled deposits are in arbitrary units).

3 Analysis & Results

Geomorphic scaling laws define consistent mathematical relationships between physical attributes of a landscape feature – for example, how the length of a feature changes relative to its area – and can serve as a powerful predictive tool even when the physical mechanisms that underpin a geomorphic system are incompletely understood (Dodds & Rothman, 2000). Geomorphic scaling laws for washover derive almost exclusively from unbuilt environments (Lazarus, 2016; Lazarus et al., 2020). Exploratory work from Hurricane Sandy on washover into a built environment found that washover scaling, specifically length relative to volume, appeared insensitive to built versus unbuilt settings: deposits in each setting tended to scale similarly, but were smaller in both length and volume in the built setting (Rogers et al., 2015). This apparent scaling insensitivity is puzzling, because field descriptions of washover deposits in built environments remark upon their distinctive shapes (Hall & Halsey, 1991; Morton & Paine, 1985; Nordstrom, 2004; Rogers et al., 2015), branching dendritically down streets and between buildings (**Fig. 2a**).

But some metrics for morphological description appear more sensitive to scaling differences than others. Here, we confirm that washover in built and unbuilt settings are effectively indistinguishable in a scaling relationship between length and area, and respective distributions of L/A (**Fig. 3a**), despite clear examples of visibly contrasting morphology in the post-storm imagery (**Fig. 2a**). A better metric for differentiation is deposit perimeter. Scaling investigations of sedimentary deposits typically omit measurements of deposit perimeter (Hudock et al., 2014; Lazarus, 2016; Moscardelli & Wood, 2016), with rare exception (Millard et al., 2017). However, unlike the scaling relationship between deposit length and area, here the relationship between perimeter and area differentiates between built and unbuilt settings (**Fig. 3b**). For a given area A, washover deposits in built environments exhibit longer perimeters than in unbuilt environments. (Note that the scaling laws that we report are nonlinear regressions of the form $y = Cx^b$ performed in linear space; results are shown plotted in log space.)

Moreover, for large areas, the perimeter data do not collapse to a single relationship: some washover deposits from built and unbuilt settings exhibit similar morphometry, while other deposits in built settings have systematically larger perimeters (**Fig. 3b**). To examine the structure within the relationship between perimeter and area, we formulated a dimensionless metric we term the distortion index (*DI*):

$$DI = \frac{P_m}{P_i} \tag{1}$$

which compares the measured perimeter (P_m) to the idealized perimeter of a semi-circle plus its diameter (P_i) with the same area as the measured deposit:

$$P_i = (\pi + 2)\sqrt{\frac{2A_m}{\pi}} \tag{2}$$

The utility of this metric is that it reflects the relative complexity of deposit perimeter as a planform path, much the way rugosity compares real to projected area to reflect the relative complexity of a surface. The perimeter of any idealized geometric shape could serve in the denominator of the distortion index, but we use a semi-circular arc (plus the diameter) since it is a common depositional fan shape, found in a range of environments (Bull, 1977; Donnelly et al., 2006; Millard et al., 2017; Moscardelli & Wood, 2016).

Applying the distortion index reveals a gradient in deposit distortion: larger deposits have the potential to become more distorted than smaller deposits (**Fig. 3b**). The distortion index is consistently higher in built settings (**Fig. 4a**). Additionally, larger deposits in built settings are more distorted than smaller deposits, relative to their unbuilt counterparts (**Fig. 4a; Fig. S3**). We further investigate the controls on the relationship between distortion index and area using the fabric of the built environment (**Fig. 4a; Fig. S1, S4, S5**). Built fabric can be described quantitatively by a host of metrics, most of which capture network properties of streets and roads (e.g., Boeing, 2020). Comprehensive analysis of built fabric in the US has shown that spatial characteristics of the built environment are heterogeneous: values of a given metric may express a narrow range, but different regions – even those broadly typified by suburban development – express different fabrics (Boeing, 2020). Here, we present results for built fraction (**Fig. 4a**), calculated as the total area of building footprints within a convex-hull bounding box around the deposit divided by the area of that hull (**Fig 2a**). We also investigated street length, calculated as the total linear length of street within the footprint of a deposit (**Fig. S4, S5**). However, for washovers that access driveways and spaces between buildings (**Fig. 2a**), a metric derived only from the street network is less descriptive of deposit distortion than a metric that reflects interaction with buildings (**Fig. S4**).

In general, we find a strong positive relationship between built fraction and deposit distortion (**Fig. 4a; Fig. S5**). In detail, we also note that for a given area *A*, deposits in the built environment can exhibit a wide range of distortion values that overlap, at the low end ($1 < DI < 1.5$), with measurements from unbuilt settings. More overlap between built and unbuilt *DI* occurs among smaller deposits: even in densely configured built settings, small deposits can form shapes similar to those of small deposits in unbuilt settings if deposition does not interact with enough of the built environment to be distorted. Several examples of overlap between built and unbuilt measurements come from Dauphin Island, Alabama, where deposition by Hurricane Nate extended into a sparsely built environment (mean built fraction = 0.038 m^2/m^2) (**Fig. 2b; Fig. S1; Table S1**). With built fraction so low, deposits by Nate in the built reach of Dauphin Island (mean $DI = 1.14$) assume almost the same morphology as deposits in the unbuilt reach (mean $DI = 1.18$). Once the built fraction locally exceeds ~0.15 m^2/m^2, deposit distortion in built and unbuilt settings appears to become more mutually distinct, as deposit morphology is forced to conform to available space prescribed by the fabric of the built environment (**Fig. 4a**).

To independently test and expand upon the scaling relationships in the empirical data, we adapted a simplified numerical model of washover deposition (Lazarus & Armstrong, 2015) to include generic fabrics using built fractions between 0–0.5 (twice the range of the empirical observations). For a given built fraction, we ran the model 25 times, with each run generating a single washover deposit from a breach imposed in the fronting dune. Initial dune height and onshore set-up were held constant, but over the 25 trials per built fraction we randomly varied breach location and depth (as a proportion of the fronting dune height) to generate washover deposits of different scales. When built fraction is low, breach depth and washover size are positively correlated. When built fraction is high, varying breach location allows some deposits to propagate down the relatively open course of a street and others to be blocked, and therefore blunted, by beach-front buildings, corroborating a previous example of a built setting reducing washover volume and extent via blocking (Rogers et al., 2015). The model is not calibrated to real length scales, but the patterns of scaling relationships generated by the model closely resemble those in the empirical data (**Fig. 4b; Fig. S6, S7**). We were able to reproduce a range of deposit sizes for a given built fraction, and a similar break in scaling between built and unbuilt settings, particularly evident as deposit area *A* increases.

4 Implications

Our empirical and modeled results indicate that the scaling relationships we derive are not storm-dependent. Rather, our findings suggest that in densely built locations, the fabric of the built environment exerts a fundamental control on the morphology of large deposits and, *ipso facto*, on pathways of overwash flow. Several factors ultimately determine the volume of an individual washover deposit in a given storm, including local availability and physical characteristics of sediment, the size and spatial heterogeneity of the fronting dune, local roughness of the terrain being overwashed, proximity to other overwash sites, storm duration, and whether the principal contribution to total water level across the barrier comes from surge or waves (e.g., Engelstad et al., 2017, 2018; Wesselman et al., 2018). Indeed, a storm may be powerful enough to overwhelm the built environment, mooting its role in steering flow and shaping deposition. Nevertheless, within the limits of a totally destructive event and despite the host of local determinants of deposit morphology, we observe that the fabric of a coastal built environment sets the conditions in which the complex morphodynamics of storm-driven sediment deposition must operate.

Given that washover deposits tend to be smaller in built relative to unbuilt settings (**Fig. 4a**), as others have noted (Rogers et al., 2015), and that deposits in built settings may or may not be recycled within the local sedimentary system (Lipton, 2013; Lazarus & Goldstein, 2019; Nordstrom, 2004), then built-environment controls on washover scale bear fundamentally on the long-term persistence of low-lying coastal barrier environments and their resilience to future hazard impacts. In more immediate terms, without understanding how much hazard-driven sediment fluxes through built environments, or knowing the anthropogenically modified pathways of that sediment, sediment budgets for developed coastlines are effectively unconstrained.

One implication of these scaling relationships and quantification of deposit distortion is that management of storm-driven sediment impacts could become less reactionary. Post-storm debris cleanup is expensive, and washover sediment constitutes a type of debris (e.g., EPA, 2019; FEMA, 2020; Nordstrom, 2004). A deposit with a larger distortion index – reflecting interaction with more of the local built environment – indicates more work for emergency-response crews. If local managers could predict washover patterns based on roads, buildings, and other fixtures of the built environment, they might more efficiently allocate financial resources for mitigating storm impacts or place limits on the maximum built fraction for a given coastal reach. Accurate prediction of washover patterns in the built environment would support the development of more sophisticated risk maps for disaster resiliency in urban planning and emergency management (Berke et al., 2006). Toward that predictive end, further research is needed to explain the complex relationship, obscured by morphodynamics, between storm intensity and washover magnitude, which remains unclear for built and unbuilt environments alike. Nevertheless, next-generation catastrophe models of storm-driven damage could soon account for the spatial patterns, and associated economic impacts, of debris clean-up – in addition to the damages from wind, waves, and surge they already consider.

We illustrate control on sediment hazard by built fabric in the context of coastal hurricanes, but the premise of our analysis extends to flow-driven hazards in tsunami, fluvial, debris-flow, and volcanic contexts. Research is beginning to demonstrate links between fabrics and socio-economic metrics as a means of informing spatial planning and urban design (Venerandi et al., 2018). Two key goals of the Sendai Framework for Disaster Risk Reduction (2015–2030) are to "reduce direct economic loss in relation to [gross domestic product]" and to "reduce disaster damage to critical infrastructure and disruption of basic services" (UN, 2015). Linking the fabric of the built environment and the physical dynamics of environments prone to flow hazards represents a tractable step toward those goals via risk assessment and mitigation – if disaster science and urban sustainability begin to account for true morphodynamics of geomorphic phenomena in built environments.

Acknowledgements

The authors gratefully acknowledge support from The Leverhulme Trust (RPG-2018-282, to EDL and EBG), DoD/DARPA (R0011836623/HR001118200064, to EBG), and an Early-Career Research Fellowship from the Gulf Research Program of the National Academies of Sciences, Engineering, and Medicine (to EBG). The content is solely the responsibility of the authors and does not necessarily represent the official views of the Gulf Research Program of the National Academies of Sciences, Engineering, and Medicine.

Data Availability

Our empirical measurements and model results are available at doi:10.6084/m9.figshare.12608828 [*link will be made live upon manuscript acceptance*]. Code for the numerical model is available at https://github.com/envidynxlab/Model-World.

Author Contributions (CRediT contributor roles)

EDL – conceptualization, investigation, methodology, formal analysis, writing, supervision, project administration, funding acquisition; *EBG* – conceptualization, investigation, methodology, formal analysis, writing, funding acquisition; *LAT* – data curation, investigation, methodology, formal analysis, writing; *HEW* – investigation, methodology, formal analysis, writing.

References

Berke, P. R., & Campanella, T. J. (2006) Planning for postdisaster resiliency. *Ann. Am. Acad. Pol. Soc. Sci.*, **604**, 192–207.

Boeing, G. (2020) A multi-scale analysis of 27,000 urban street networks: every US city, town, urbanized area, and Zillow neighborhood. *Environ. Plann. B.*, **47**, 590–608.

Bricker, J. D., Gibson, S., Takagi, H., & Imamura, F. (2015) On the need for larger Manning's roughness coefficients in depth-integrated tsunami inundation models. *Coast. Eng. J.* **57**, https://doi.org/10.1142/S0578563415500059.

Brown, C., Milke, M., & Seville, E. (2011) Disaster waste management: a review article. *Waste Manage.*, **31**, 1085–1098.

Bull, W. B. (1977) The alluvial-fan environment. *Prog. Phys. Geog.*, **1**, 222–270.

Del Ventisette, C., Garfagnoli, F., Ciampalini, A., Battistini, A., Gigli, G., Moretti, S., & Casagli N. (2012) An integrated approach to the study of catastrophic debris-flows: geological hazard and human influence. *Nat. Hazards Earth Syst. Sci.*, **12**, 2907–2922 (2012).

Dodds, P. S., & Rothman, D. H. (2000) Scaling, universality, and geomorphology. *Annu. Rev. Earth Planet. Sci.*, **28**, 571–610.

Donnelly, C., Kraus, N., & Larson, M. (2006) State of knowledge on measurement and modeling of coastal overwash. *J. Coastal Res.*, **22**, 965–991.

Doronzo, D. M., & Dellino, P. (2011) Interaction between pyroclastic density currents and buildings: numerical simulation and first experiments. *Earth Planet. Sc. Lett.*, **310**, 286–292.

Ellis, E. C., Ramankutty, N. (2008) Putting people in the map: anthropogenic biomes of the world. *Front. Ecol. Environment.*, **6**, 439–447.

Engelstad, A., Ruessink, B. G., Wesselman, D., Hoekstra, P., Oost, A., & van der Vegt, M. (2017) Observations of waves and currents during barrier island inundation. *J. Geophys. Res.-Oceans*, **122**, 3152–3169.

Engelstad, A., Ruessink, B. G., Hoekstra, P., & van der Vegt, M. (2018) Sand suspension and transport during inundation of a Dutch barrier island. *J. Geophys. Res.-Earth*, **123**, 3292–3307.

EM-DAT: The Emergency Events Database (Université Catholique de Louvain [UCL]–Centre for Research on the Epidemiology of Disasters [CRED], Brussels, Belgium, 2019). Retrieved from http://www.emdat.be (accessed July 2020).

Environmental Protection Agency (EPA), Planning for natural disaster debris, EPA 530-F-19-003 (2019). Retrieved from https://www.epa.gov/sites/production/files/2019-04/documents/final_pndd_guidance_0.pdf (accessed July 2020).

Federal Emergency Management Agency [FEMA] (2020), Public Assistance Program and Policy Guide (Version 4), FP 104-009-2.

FitzGerald, D. M., Fenster, M. S., Argow, B. A., & Buynevich, I. V. (2008) Coastal impacts due to sea-level rise. *Annu. Rev. Earth Pl. Sc.*, **36**, 601–647.

Foley, J. A., DeFries, R., Asner, G. P., Barford, C., Bonan, G., Carpenter, S. R., *et al.* (2005) Global consequences of land use. *Science*, **309**, 570–574.

Gurioli, L., Pareschi, M. T., Zanella, E., Lanza, R., Deluca, E., & Bisson, M. (2005) Interaction of pyroclastic density currents with human settlements: evidence from ancient Pompeii. *Geology*, **33**, 441–444.

Gurioli, L., Zanella, E., Pareschi, M. T., & Lanza, R. (2007) Influences of urban fabric on pyroclastic density currents at Pompeii (Italy): 1. Flow direction and deposition. *J. Geophys. Res-Solid*, **112**, B05213.

Hall, M. J., & Halsey, S. D. (1991) Comparison of overwash penetration from Hurricane Hugo and pre-storm erosion rates for Myrtle Beach and North Myrtle Beach, South Carolina, U.S.A. *J. Coast. Res.*, **SI 8**, 229–235.

Halpern, B. S., Frazier, M., Potapenko, J., Casey, K. S., Koenig, K., Longo, C., *et al.* (2015) Spatial and temporal changes in cumulative human impacts on the world's ocean. *Nat. Commun.*, **6**, 7615.

Hudock, J. W., Flaig, P. P., & Wood, L. J. (2014) Washover fans: a modern geomorphologic analysis and proposed classification scheme to improve reservoir models. *J. Sediment. Res.*, **84**, 854–865.

Lipton, E. (2013) Cost of storm-debris removal in city is at least twice the U.S. average. New York *Times* (25 April 2013). Retrieved from https://www.nytimes.com/2013/04/25/nyregion/debris-removal-from-hurricane-sandy-is-more-costly-than-average.html (accessed July 2020).

UN General Assembly (2015) The Sendai Framework for Disaster Risk Reduction 2015-2030. Retrieved from http://www.unisdr.org/files/43291_sendaiframeworkfordrren.pdf (accessed July 2020).

Grinsted, A., Ditlevsen, P., & Christensen, J. H. (2019) Normalized US hurricane damage estimates using area of total destruction, 1900–2018. *P. Natl. Acad. Sci. USA*, **116**, 23942–23946.

Kossin, J. P., Knapp, K. R., Olander, T. L., & Velden, C. S. (2020) Global increase in major tropical cyclone exceedance probability over the past four decades. *Proc. Natl. Acad. Sci. USA*, **117**, 11975–11980.

Lazarus, E. D. (2016) Scaling laws for coastal overwash morphology. *Geophys. Res. Lett.*, **43**, 113–119.

Lazarus, E. D., & Armstrong, S. (2015) Self-organized pattern formation in coastal barrier washover deposits. *Geology*, **43**, 363–366.

Lazarus, E. D., Davenport, K. L., & Matias, A. (2020) Dynamic allometry in coastal overwash morphology. *Earth Surf. Dynam.*, **8**, 37–50.

Lazarus, E. D., & Goldstein, E. B. (2019) Is there a bulldozer in your model? *J. Geophys. Res.-Earth*, **124**, 696-699.

Leatherman, S. P., & Zaremba, R. E. (1987) Overwash and aeolian processes on a U.S. northeast coast barrier. *Sediment. Geol.*, **52**, 183–206.

Masselink, G., & van Heteren, S. (2014) Response of wave-dominated and mixed-energy barriers to storms. *Mar. Geol.*, **352**, 321–347.

Matias, A., Vila-Concejo, A., Ferreira, O., Morris, B., & Dias, J. A. (2009) Sediment dynamics of barriers with frequent overwash. *J. Coastal Res.*, **25**, 768–780.

Millard, C., Hajek, E., & Edmonds, D. A. (2017) Evaluating controls on crevasse-splay size: implications for floodplain-basin filling. *J. Sediment. Res.*, **87**, 722–739.

Morton, R. A., & Paine, J. G. (1985) Beach and vegetation-line changes at Galveston Island, Texas: erosion, deposition and recovery from Hurricane Alicia. Bureau of Economic Geology, Geological Circular 85-5.

Morton, R. A., & Sallenger, A. H. (2003) Morphological impacts of extreme storms on sandy beaches and barriers. *J. Coastal Res.*, **19**, 560–573.

Moscardelli, L., & Wood, L. (2016) Morphometry of mass-transport deposits as a predictive tool. *GSA Bulletin*, **128**, 47-80.

National Geodetic Survey. Emergency response imagery. Retrieved from https://storms.ngs.noaa.go (accessed July 2020).

National Oceanic and Atmospheric Administration [NOAA] (2013) National Coastal Population Report: State of the Coast.

Nelson, S. A., & Leclair, S. F. (2006) Katrina's unique splay deposits in a New Orleans neighbourhood. *GSA Today*, **16**, 4–10.

Nordstrom, K. F. (2004) Beaches and dunes of developed coasts. Cambridge University Press.

Overbeck, J. R., Long, J. W., Stockdon, H. F., & J. J. Birchler (2015) Enhancing evaluation of post-storm morphologic response using aerial orthoimagery from Hurricane Sandy, in *Coastal Sediments 2015,* edited by P. Wang, J. D. Rosati, World Scientific, Miami, Fla.

Papathoma-Köhle, M., Gems, B., Sturm, M., & Fuchs, S. (2017) Matrices, curves and indicators: a review of approaches to assess physical vulnerability to debris flows. *Earth-Sci. Rev.*, **171**, 272–288.

Park, H., Cox, D. T., Lynett, P. J., Wiebe, D. M., & Shin, S. (2013) Tsunami inundation modeling in constructed environments: a physical and numerical comparison of free-surface elevation, velocity, and momentum flux. *Coast. Eng.*, **79**, 9–21.

Periathamby, A., Hamid, F. S., & Sakai, S. (2012) Disaster waste management challenges. *Waste Manage. Res.*, **30**, 113–114.

Rogers, L. J., Moore, L. J., Goldstein, E. B., Hein, C. J., Lorenzo-Trueba, J., & Ashton, A. D. (2015) Anthropogenic controls on overwash deposition: evidence and consequences. *J. Geophys. Res.-Earth*, **120**, 2609–2624.

Sallenger, J. (2000) Storm impact scale for barrier islands. *J. Coast. Res.*, **16**, 890–895.

Serafin, K. A., Ruggiero, P., & Stockdon, H. F. (2017) The relative contribution of waves, tides, and nontidal residuals to extreme total water levels on U.S. West Coast sandy beaches. *Geophys. Res. Lett.*, **44**, 1839–1847.

Shaw, J., You, Y., Mohrig, D., & Kocurek, G. (2015) Tracking hurricane-generated storm surge with washover fan stratigraphy. *Geology*, **43**, 127–130.

Smallegan, S. M., Irish, J. L. (2017) Barrier island morphological change by bay-side storm surge. *J. Waterw. Port. C. Div.*, **143**, https://doi.org/10.1061/(ASCE)WW.1943-5460.0000413.

USGS (2005) Pre- and post-storm 3D Topography: Dauphin Island. Retrieved from https://coastal.er.usgs.gov/hurricanes/katrina/lidar/dauphin-island.html (accessed July 2020).

Venerandi, A., Quattrone, G., & Capra, L. (2018) A scalable method to quantify the relationship between urban form and socio-economic indexes. *EPJ Data Science*, *7*, 1–21.

Venter, O., Sanderson, E. W., Magrach, A., Allan, J. R., Beher, J., Jones, K. R., *et al.* (2016) Sixteen years of change in the global terrestrial human footprint and implications for biodiversity conservation. *Nat. Commun.*, **7**, 12558.

Vitousek, P. M., Mooney, H. A., Lubchenco, J., & Melillo, J. M. (1997) Human domination of the Earth's ecosystems. *Science*, **277**, 494–499.

Wesselman, D., de Winter, R., Engelstad, A., McCall, R., van Dongeren, A., Hoekstra, P., *et al.* (2018) The effect of tides and storms on the sediment transport across a Dutch barrier island. *Earth Surf. Process. Landforms*, **43**, 579–592.

Zanella, E., Gurioli, L., Pareschi, M. T., Lanza, R. (2007) Influences of urban fabric on pyroclastic density currents at Pompeii (Italy): 2. Temperature of the deposits and hazard implications. *J. Geophys. Res-Solid*, **112**, B05214.

Figures & Captions

Figure 1. Excavators (circled and detailed) clearing washover sand from the main road along Dauphin Island, Alabama, 10 October 2017, two days after Hurricane Nate. (Location marker *x*: 30º15'03"N, 88º10'77"W.) Image courtesy of NOAA.

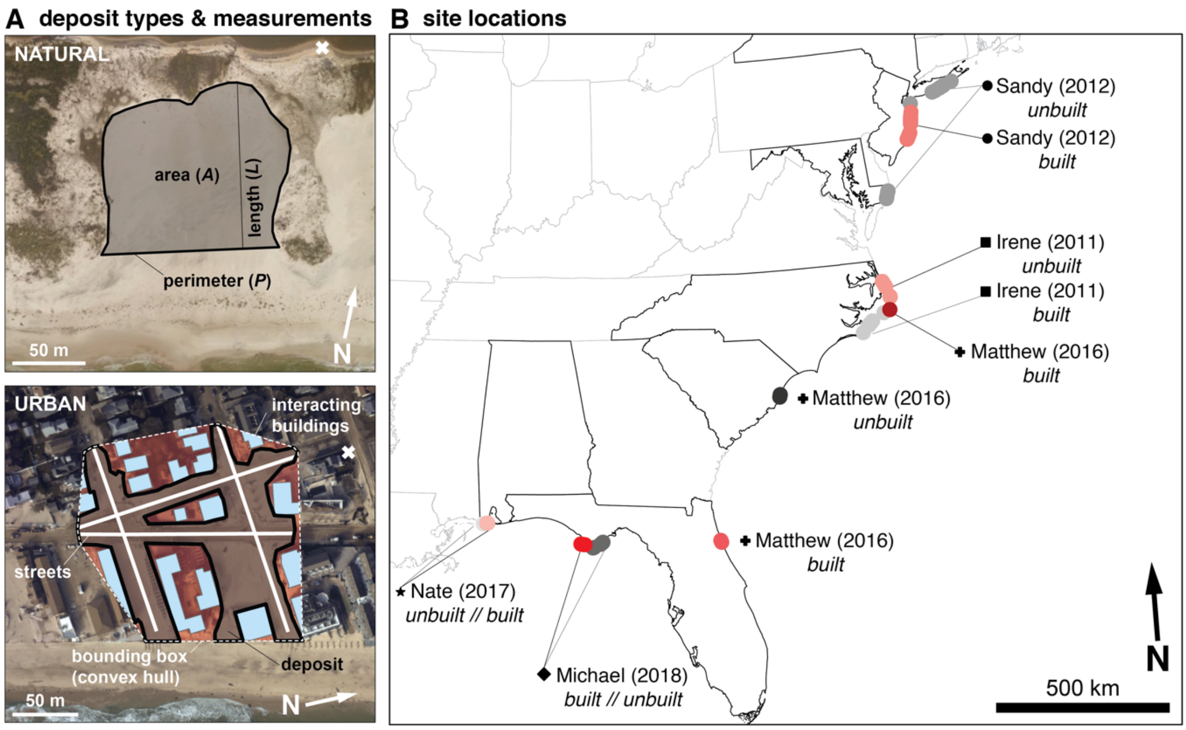

502

503 **Figure 2.** Hurricane deposition in comparative settings. **(*A*)** Illustrative comparison of washover
504 in unbuilt (upper panel; location marker *x*: 30°14'5"N, 88°16'55"W) and built environments
505 (lower panel; location marker *x*: 40°5'19"N, 74°2'22"W), showing washover geometry and built
506 fabric we use in this analysis. Deposit in upper panel is from Dauphin Island, Alabama,
507 following Hurricane Nate (2017); deposit in lower panel is from Point Pleasant Beach, New
508 Jersey, following Hurricane Sandy (2012). Images courtesy of NOAA. **(*B*)** Map of washover
509 sampling locations by hurricane and setting type. Shades of red indicate relative built fraction.
510 Data distributions of built fraction by location are provided in **Fig. S1**.

511

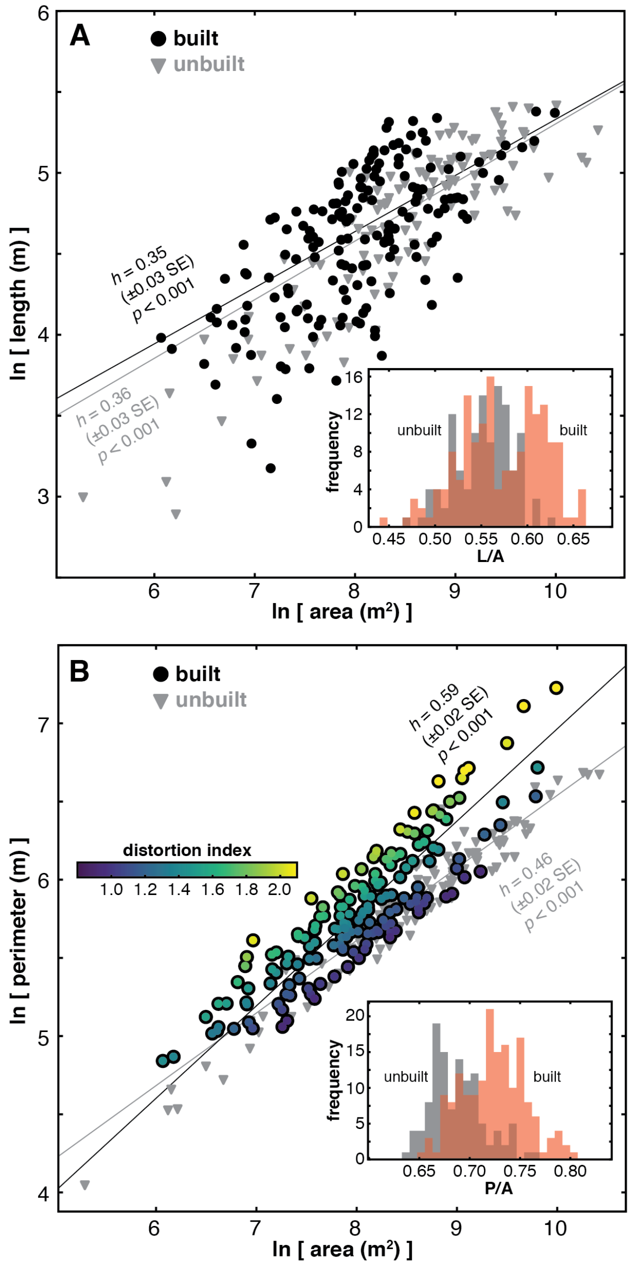

Figure 3. Scaling relationships for washover deposits in built and unbuilt settings. **(*A*)** Washover length relative to area from built (black circles) and unbuilt settings (gray triangles). Inset shows relative distributions of length-to-area ratio for the two types of setting. The closely overlapping distributions in this relationship make any morphological differences between the two settings difficult to discern. **(*B*)** Washover perimeter relative to area from built (black circles) and unbuilt settings (gray triangles); inset shows relative distributions of the perimeter-to-area ratio. This relationship shows a clearer distinction in washover morphology from the two types of setting. Color gradient superimposed on the built-setting data shows the distortion index (*DI*) of each data point, or the degree to which the perimeter deviates from the perimeter of an idealized semi-circle of the same area, and indicates a further dimension of organization embedded in the perimeter-to-area relationship. Nonlinear regressions of the form $y = Cx^h$ were performed in linear space; results are plotted in log space. Summary statistics are provided in **Table S1**, and additional plots of comparative data distributions in **Fig. S2**.

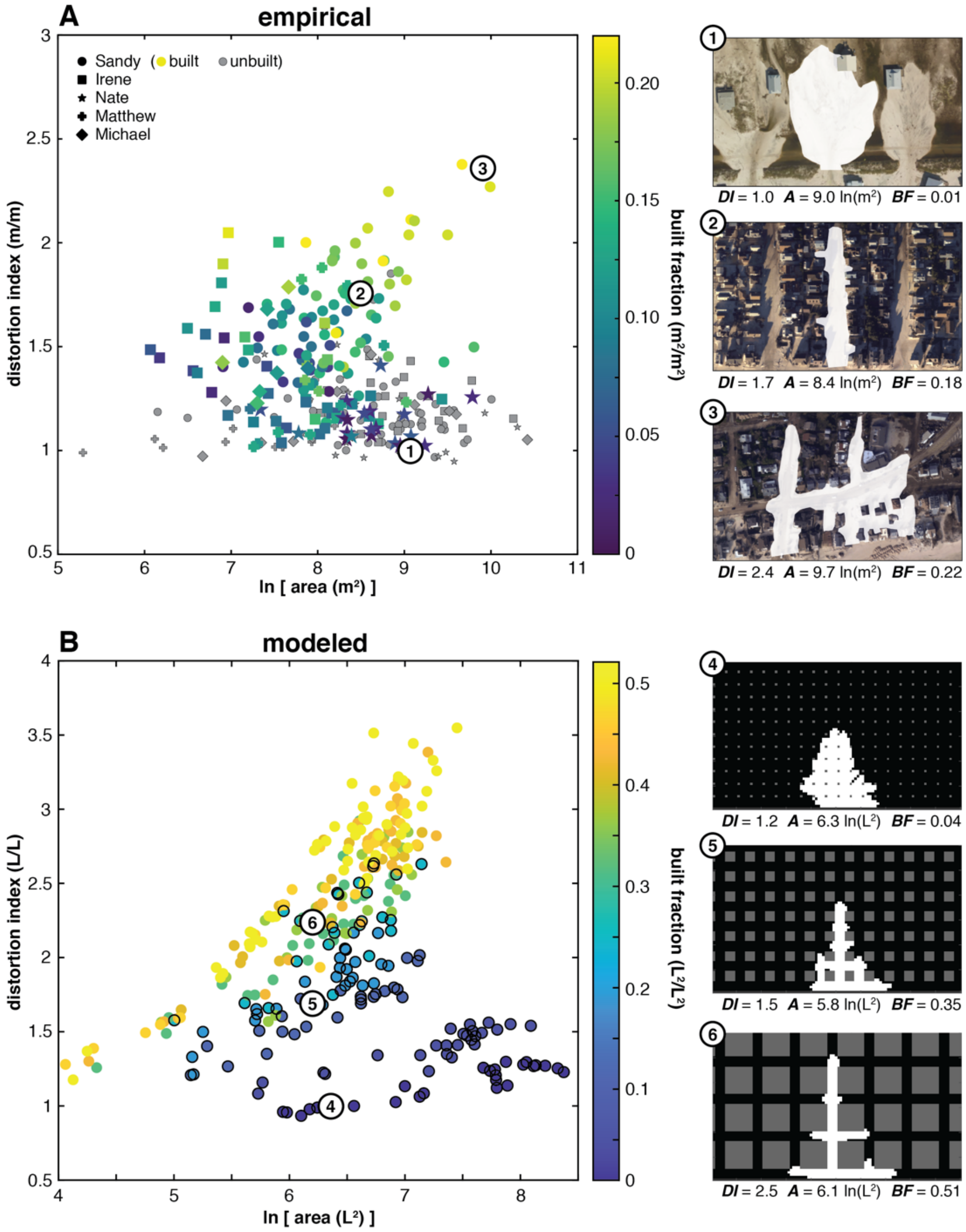

Figure 4. Distortion index (*DI*) as a measure of washover interaction with the built environment. **(*A*)** Distortion index as a function of area, for the empirical data. Color gradient represents built fraction; symbols indicate the hurricane event in which the deposit formed. Gray symbols (with fine black outline) indicate washover measurements from unbuilt settings. Illustrative examples of different deposit morphologies are shown at right: (1) low *DI*, from Dauphin Island, Alabama, after Hurricane Nate; (2) medium *DI*, from Seaside Park, New Jersey, after Hurricane Sandy; and (3) high *DI*, from Bay Head, New Jersey, after Hurricane Sandy. Images from NOAA. **(*B*)** Distortion index as a function of area, from a simplified numerical model of washover deposition into built environments. Color gradient represents built fraction; circled data points indicate the range of built fractions (< 0.25) captured by the empirical data in (*A*). Illustrative examples from modeled deposits with (4) low, (5) medium, and (6) high *DI* are shown at right. Additional comparisons are shown in **Fig. S1, S6 and S7**.

SUPPORTING INFORMATION **APPENDIX FOR:**

Comparing patterns of hurricane washover into built and unbuilt environments

Eli D. Lazarus[a1], Evan B. Goldstein[b1], Luke A. Taylor[a], Hannah E. Williams[a]

[a]Environmental Dynamics Lab, School of Geography and Environmental Science, University of Southampton, Southampton, SO17 1BJ, UK

[b]Department of Geography, Environment, and Sustainability, University of North Carolina at Greensboro, Greensboro, NC, USA

ORCiDs:

EDL: 0000-0003-2404-9661

EBG: 0000-0001-9358-1016

LAT: 0000-0002-2132-4261

HEW: 0000-0002-6143-2523

Correspondence to – Eli D Lazarus (E.D.Lazarus@soton.ac.uk), Evan B Goldstein (ebgoldst@uncg.edu)

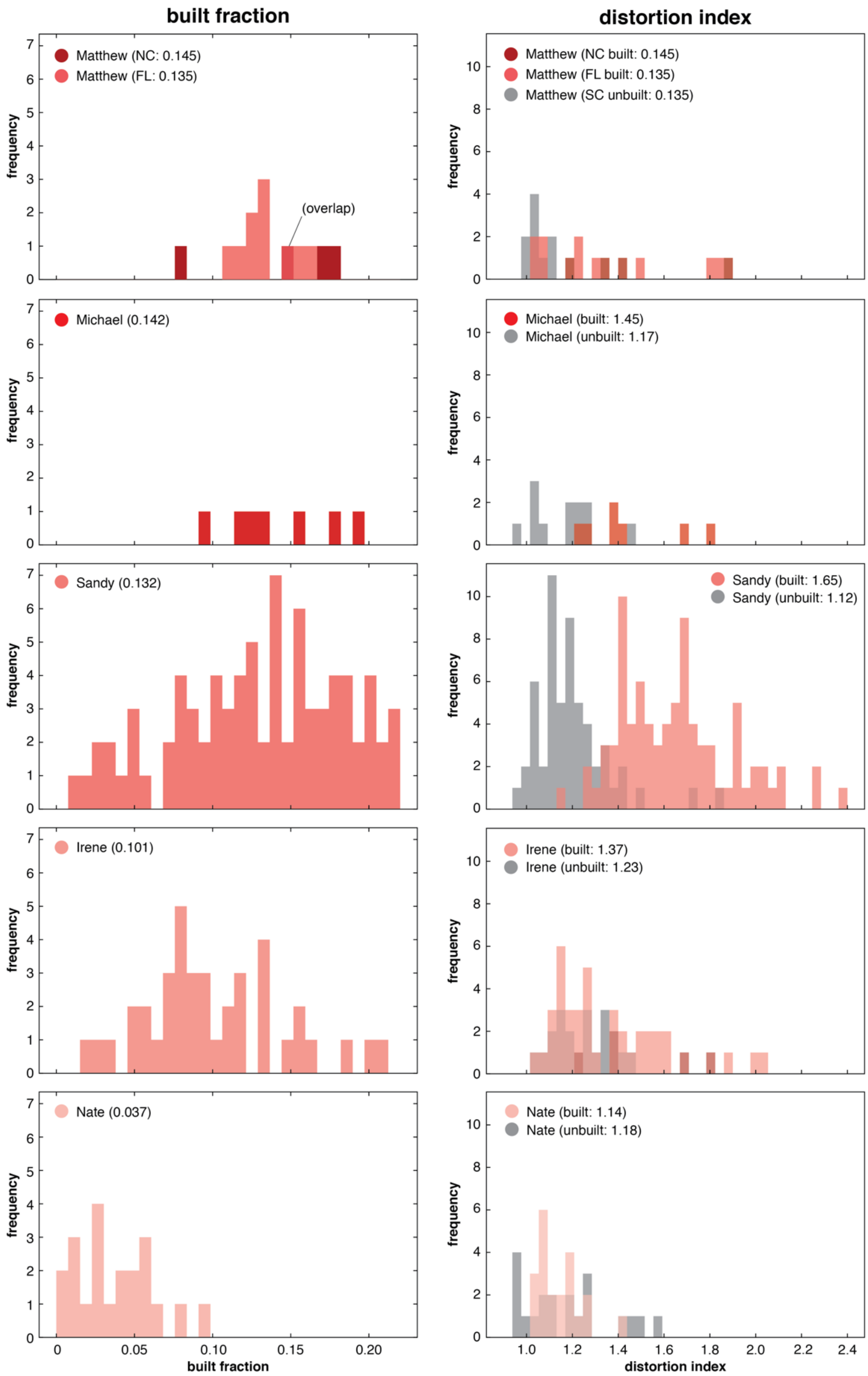

Figure S1. Distributions of built fraction (left) and distortion index (right) by hurricane event. Color gradients are based on relative built fraction, and correspond to map in **Fig. 2b**. Distributions of distortion index include deposits from both built (red shades) and unbuilt (gray) settings from each hurricane.

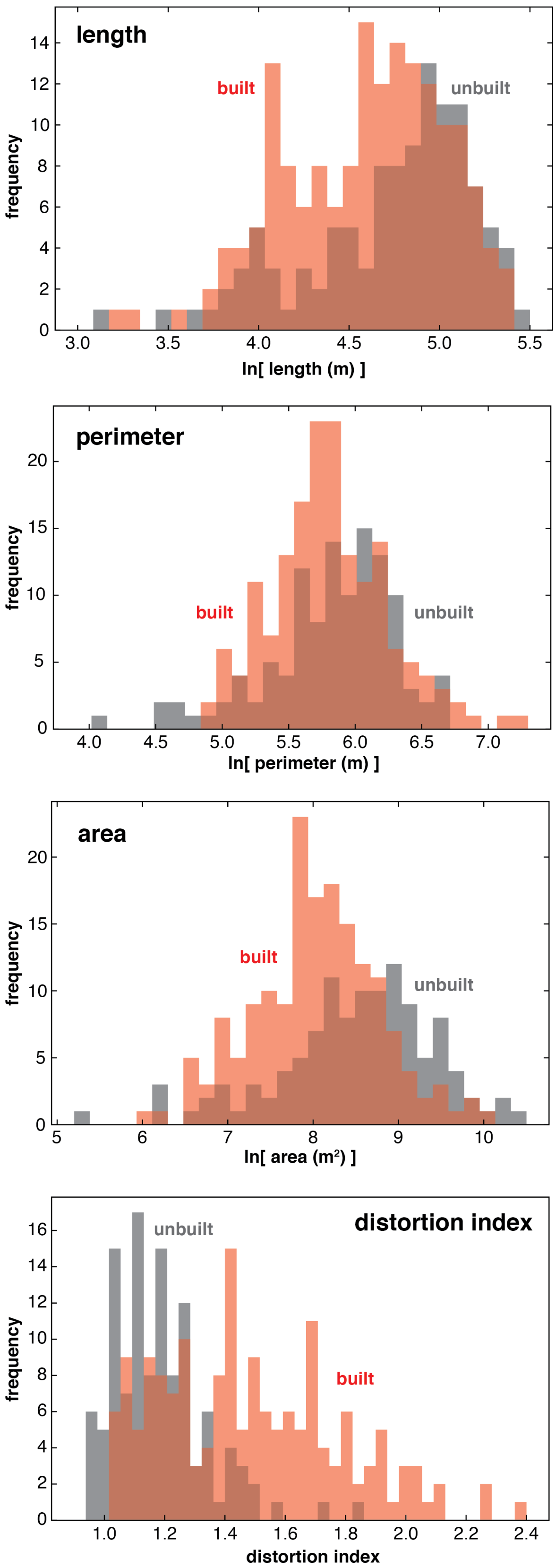

Figure S2. Comparative distributions of length, perimeter, area, and distortion index for all deposits from built (red) and unbuilt (gray) settings, respectively. Length, perimeter, and area are plotted in log-transform space.

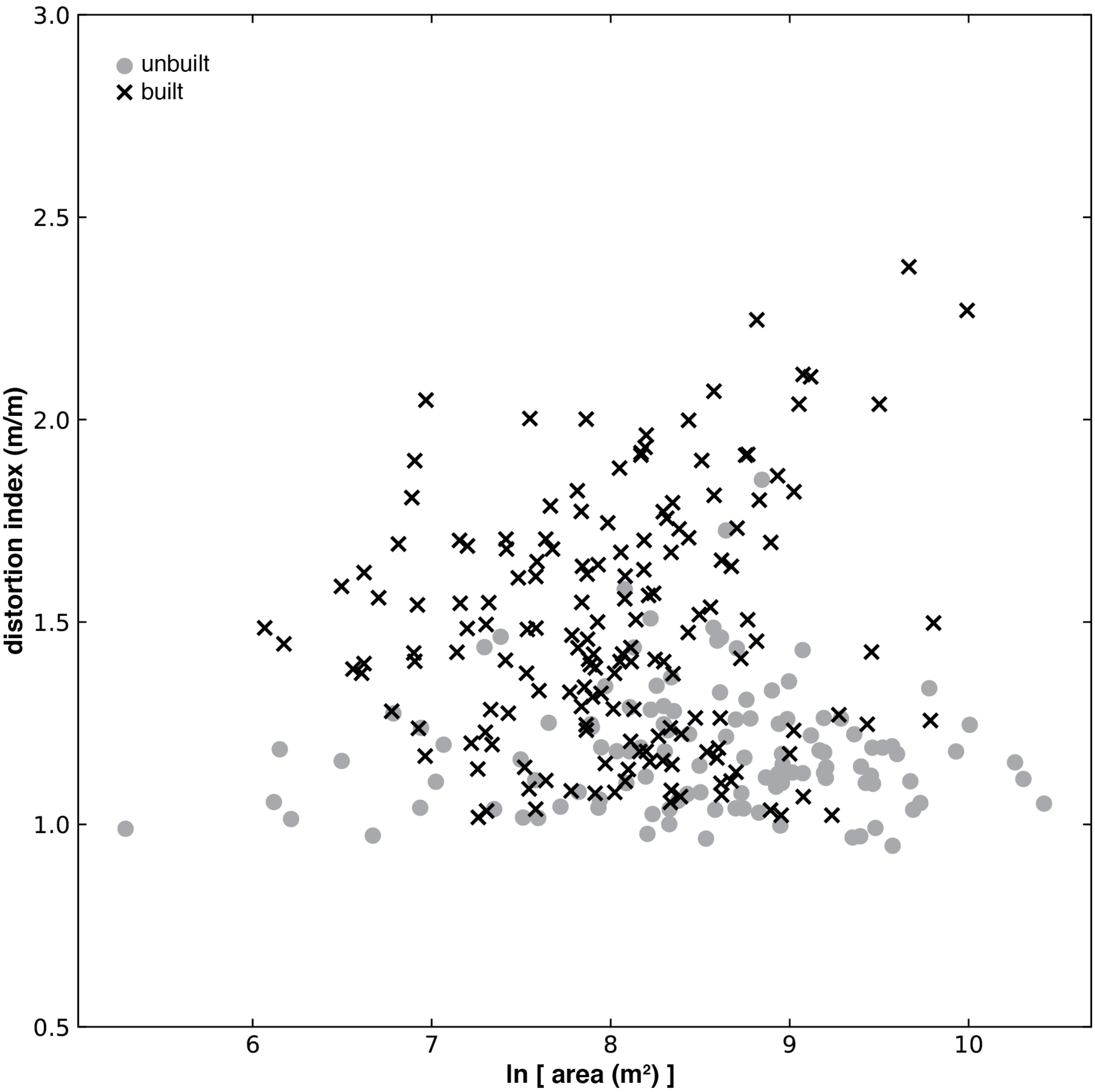

Figure S3. Distortion index as a function of area for deposits from built (black x) and unbuilt (gray circles) settings, undifferentiated by storm event.

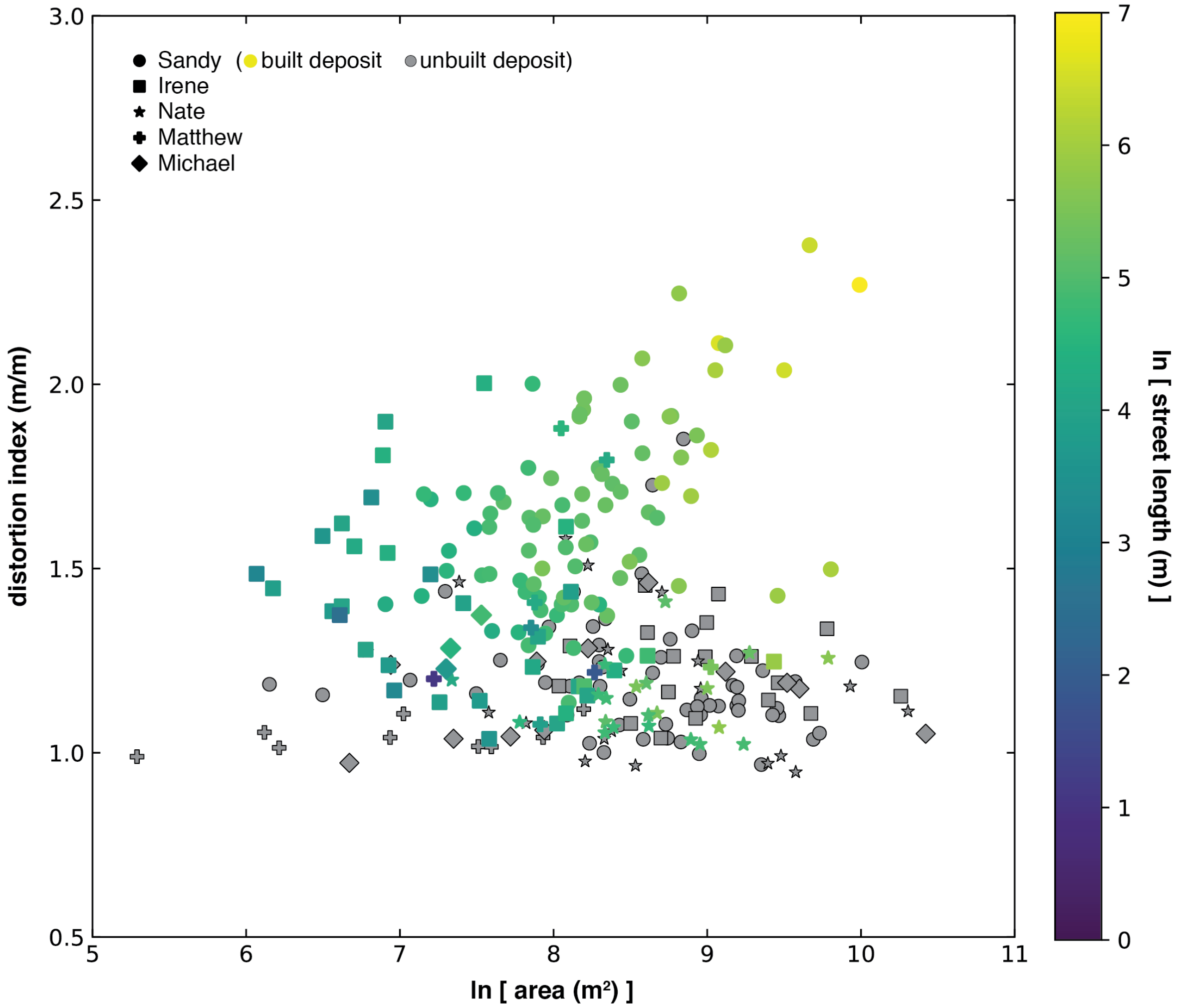

Figure S4. Distortion index as a function of area. Color gradient represents total street length (within the footprint of a given deposit). Symbols indicate the hurricane event in which the deposit formed. Gray symbols indicate washover measurements from unbuilt settings. The color gradient is more lateral than vertical, indicating that street length is more sensitive to overall deposit area than to deposit distortion.

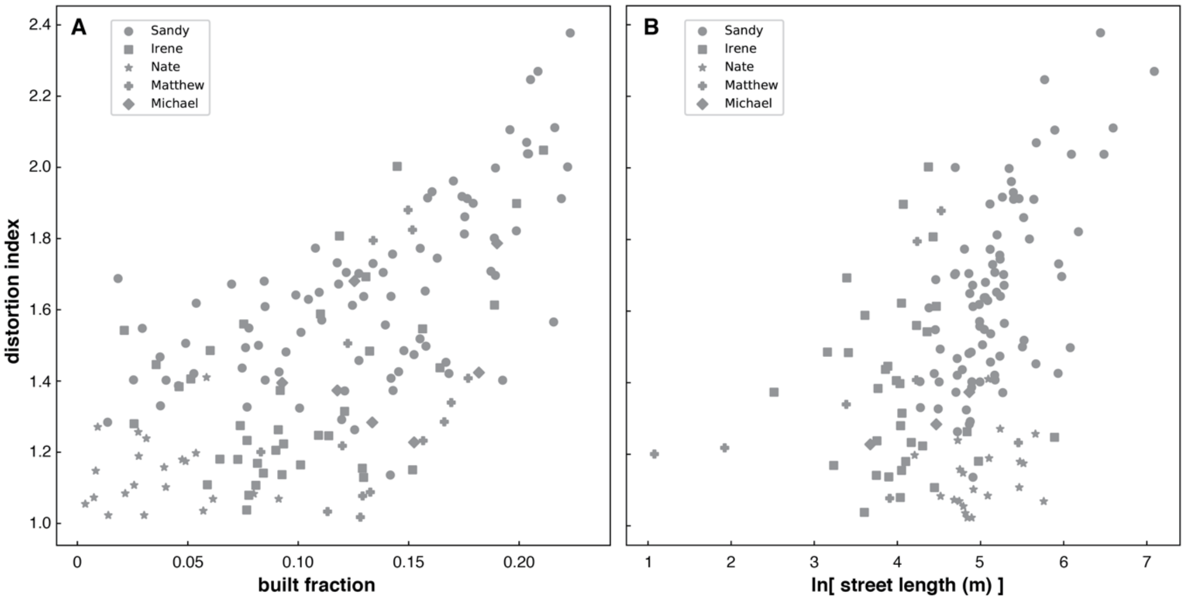

Figure S5. Distortion index plotted as a function of ***(A)*** built fraction and ***(B)*** street length. Symbols indicate the hurricane event in which the deposit formed.

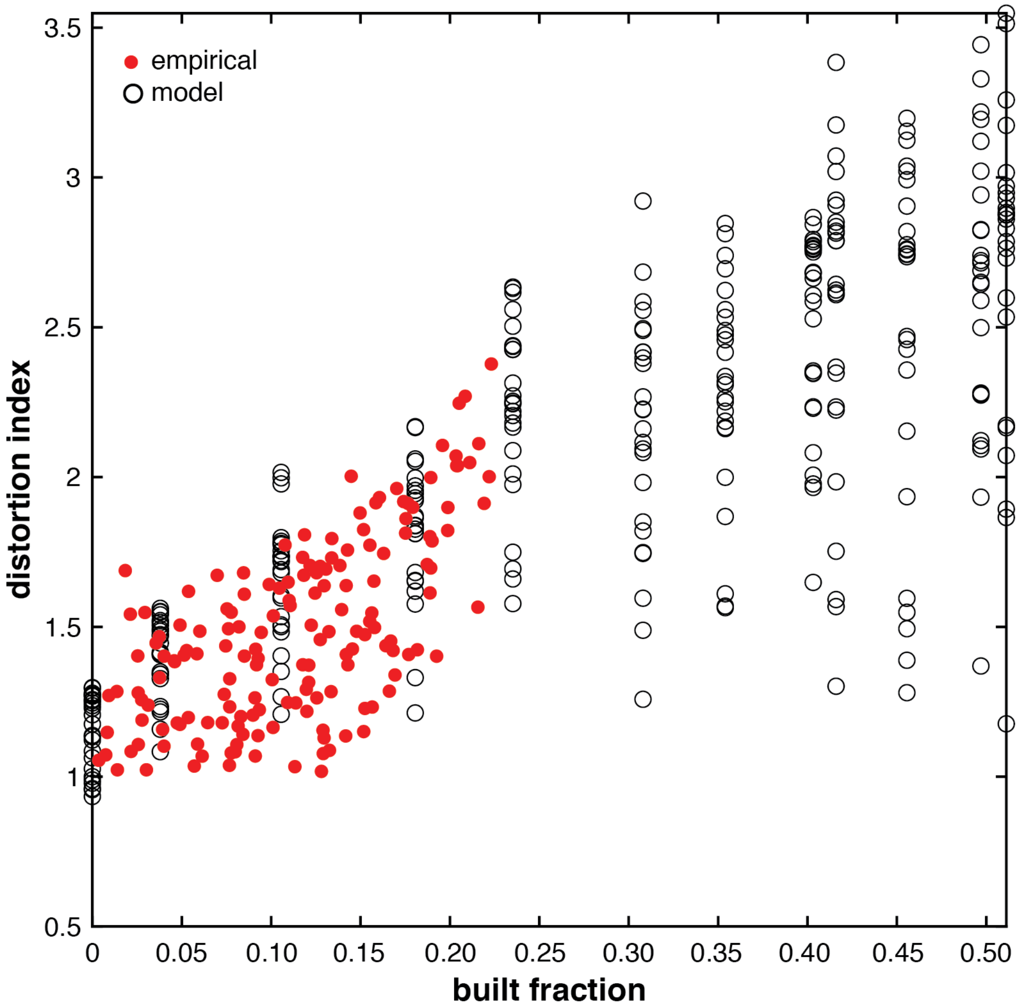

Figure S6. Distortion index plotted as a function of built fraction, for empirical (red dots) and modeled results (open circles). The numerical model explores a range of hypothetical built fractions approximately twice that observed in the empirical data.

Please note that this is a non-peer-reviewed EarthArXiv preprint

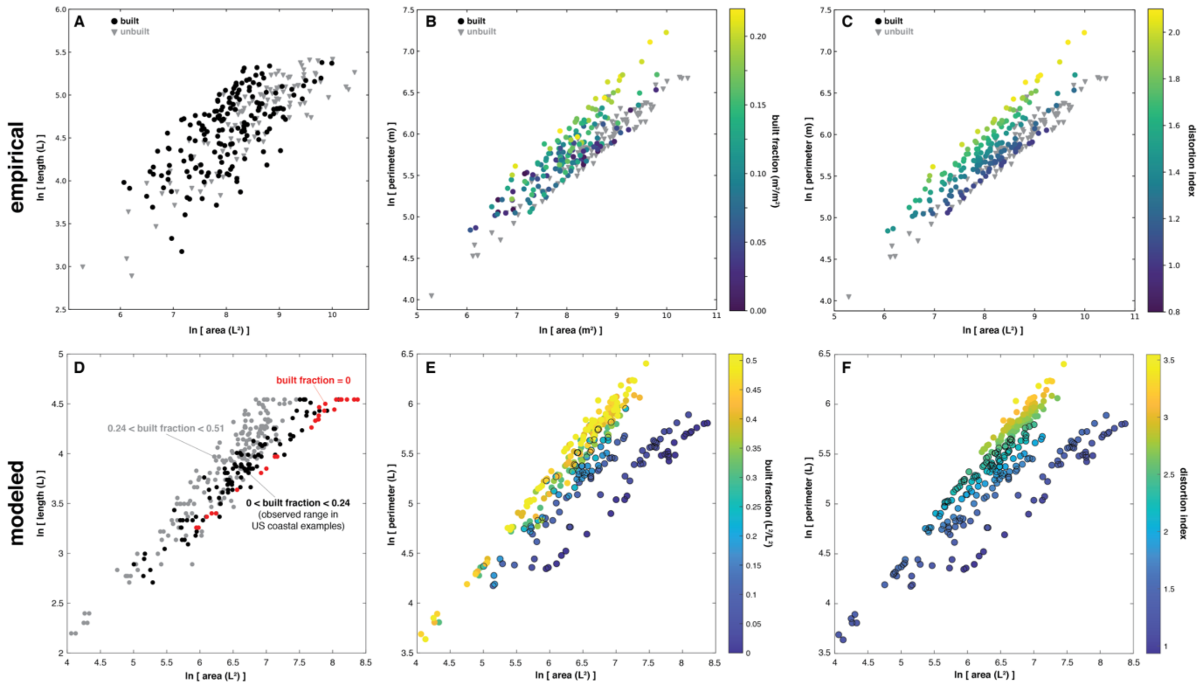

Figure S7. Comparative scaling relationships for length to area, perimeter to area by built fraction, and perimeter to area by distortion index for the empirical (top row) and modeled results (bottom row). In panels (*E*) and (*F*), outlined circles indicate ranges of built fraction and distortion index, respectively, represented in the empirical data.

Table S1. Summary statistics for data presented in main article.

Hurricane	Landfall	Imagery Dates	Deposits – built (#)	Deposits – unbuilt (#)
Sandy	29 Oct 2012	31 Oct, 1 Nov	83	56
Nate	7 Oct 2017	10 Oct	21	20
Michael	10 Oct 2018	11, 14 Oct	7	12
Matthew (FL)	7 Oct 2016	9 Oct	10	-
Matthew (NC)	7 Oct 2016	10 Oct	4	-
Matthew (SC)	7 Oct 2016	9 Oct	-	9
Irene	27 Aug 2011	28 Aug	42	18
		total	**167**	**115**

Corresponds to locations shown in **Fig. 2b**.

Setting	Relationship	Scaling exponent *h*	Standard Error (*h*)	Coefficient *C*	Standard Error (*C*)	*p* value
unbuilt	*L* v *A*	0.362	0.0273	5.379	1.329	< 0.001
built	*L* v *A*	0.347	0.0315	6.448	1.714	< 0.001
unbuilt	*P* v *A*	0.464	0.0154	6.683	0.94	< 0.001
built	*P* v *A*	0.591	0.0246	2.883	4.682	< 0.001

Corresponds to scaling relationships of forms $L = C{*}A^h$ and $P = C{*}A^h$ shown in **Fig. 3**.

setting	BUILT				UNBUILT	
Hurricane	**mu *BF***	**stdv *BF***	**mu *DI***	**stdv *DI***	**mu *DI***	**stdv *DI***
Sandy	0.13	0.06	1.65	0.25	1.20	0.16
Nate	0.04	0.02	1.14	0.01	1.18	0.19
Michael	0.14	0.04	1.45	0.21	1.17	0.14
Matthew (FL)	0.14	0.02	1.31	0.30	-	-
Matthew (NC)	0.15	0.04	1.46	0.30	-	-
Matthew (SC)	-	-	-	-	1.04	0.04
Irene	0.10	0.05	1.37	0.25	1.23	0.12

Mean built fraction (*mu BF*), standard deviation of the built fraction (*stdv BF*), mean distortion index (*mu DI*), and standard deviation of the distortion index (*stdv DI*) for each location shown in **Fig. 2b**.